Automated Kidney Cancer Classification using White Shark Optimizer with Ensemble Majority Voting Model on Pathology Images

Ashrf Althbiti[1,*]

[1]Department of Information Technology, College of Computers and Information Technology, Taif University, Taif, 21944, Saudi Arabia

Email: a.althbiti@tu.edu.sa

Abstract

Kidney cancer is a lethal cancerous and very dangerous disease caused by genetic renal disease or by kidney tumors, and some patients might survive since there is no technique for earlier diagnosis of kidney tumor. Earlier diagnosis of kidney tumor assists physicians to begin proper treatment and therapy for the patient, which prevent kidney cancers and renal transplantation. Accurate classification of kidney tumor is vital for prediction and treatment planning. However, manual classification by pathologists could be subjective and time-consuming, and there can be considerable inter-observer variability. With the development of artificial intelligence (AI), automated tools enabled by machine learning (ML) and deep learning (DL) methods could predict cancers. This study designs a new white shark optimizer with an ensemble majority voting based kidney cancer classification (WSO-EMVKCC) technique on pathology images. The presented WSO-EMVKCC technique intends to identify the different grades of kidney cancer using DL and ensemble voting concepts. To accomplish this, the presented WSO-EMVKCC technique employs a deep convolutional neural network based Xception technique for the feature extraction process. Moreover, the WSO model has been used for the optimal hyperparameter tuning of the Xception approach. Furthermore, an ensemble majority voting classifier including three ML techniques like long short-term memory (LSTM), sparse autoencoder (SAE), and gated recurrent unit (GRU) models are employed for kidney cancer classification. The stimulation validation of the WSO-EMVKCC model is performed on the open access histology image database from Kaggle repository. The stimulated values illustrate the promising performance of the WSO-EMVKCC algorithm over other DL techniques.

Keywords: Kidney cancer classification; Deep learning; Ensemble models; Majority voting; White shark optimizer

1. Introduction

Kidney cancer is a lethal and extremely dangerous disease caused by genetic renal disease and survival rate of patients is lesser due to lack of proper treatment and technique for initial prediction of kidney tumor [1]. Initial diagnosis of kidney tumor aids clinicians start correct treatment and prognosis for the patient, which prevents renal transplantation and kidney cancers. Automatic tools enabled with deep learning (DL) and machine learning (ML) techniques can predict tumors by adopting artificial intelligence (AI) [2].

To avoid inessential surgery or biopsy, it is vital to precisely distinguish benign and malignant ones in preoperative images [3]. In addition, as prognosis prediction and treatment planning are high dependent on the pathological subtypes of renal cancer, it should accurately categorize cancer sub-types in images. To confirm detection and classification of kidney and other kinds of cancer a technique called Histopathology is considered a well-established method. This method contains the graphical study of microscopic slides gained in tissue models commonly stained with haematoxylin and eosin stains (H&E) [4]. This task is time taking and not an appropriate

DOI: https://doi.org/10.54216/FPA.190230
Received: September 14, 2024 Revised: February 02, 2025 Accepted: March 03, 2025

method even though skilled experts [5] carry it out. Along with that, in kidney and other tumours, histological analysis usage for the diagnosis purpose is always a challenge as various cancer sub-types might share non-specific morphological paradigms [6]. Hence, the robust and accurate analysis of huge volume of digitalized histological slides for cancer diagnosis is main difficulty in clinical practice and cancer research.

Earlier studies on the image-based quantitative classification of renal masses have focused on distinguishing benign and malignant lesions from normal kidneys [7]. On the other hand, the next plausible step in this domain learning how to differentiate the malignant sub kinds of the renal masses, as image features of various Renal cell carcinoma (RCC) subtypes are utilized to forecast overall prognosis, clinical behavior, and treatment response [8]. On top of that, the non-invasive diagnosis may be useful, especially for elderly patients having small masses. One of the powerful ML technologies is DL, which could automatically study multiple patterns and features without intervention of humans. DL allowed the building of prediction methods for the initial diagnosis of cancer, and experts utilized proven pattern analysis approaches [9]. DL techniques exceed conventional ML because of their outcomes with higher levels of accuracy. Similarly, it surpasses or matches the performance of humans. So, they are suggested as the optimal technique to manage the images. It has received considerable benefit in image processing, specifically in the health care sector, as radiology is mainly concerned with extraction of valuable data from images [10].

A. Existing Works on Kidney Cancer Classification

Alzu'bi et al. [11] presented detection approaches to diagnose the kidney tumour (KT) in Computed Tomography (CT) scans. Towards the classification and detection of the KT, the author devised 2D convolutional neural network (CNN) methods; 3 approaches are considering KT detection like a VGG16 with 16 layers, 2D CNN with six layers, and a ResNet50 having 50 layers. In [12], this presented technique employed the Internet of Medical Things (IoMT)-based TL approach adds various DL approaches to forecast KT at its initial level and for the data security of patients, this method-incorporated blockchain (BC) technology-based TL trained models and private clouds. This algorithm leveraged biopsies of tumorous kidneys comprising 3 classes for forecasting KT.

Shon et al. [13] introduced a method named COST-HDL (cost-sensitive hybrid DL) with cost-sensitive loss function for classifier tasks on imbalanced KT dataset. In this study, the author compiled the deep symmetric autoencoder (AE); the decoders are symmetric to encoders in the context of layer structure, with reconstructed loss for nonlinear feature extracting process and NN having balanced classification loss for diagnosis estimation for solving data imbalance issues. In [14], devised a Heterogeneous Modified Artificial neural network (HMANN) for initial recognition, segmentation, and detection of chronic renal failure in IoMT environment. On top of that, this HMANN was classified as Multilayer Perceptron (MLP) and Support vector machine (SVM) with Backpropagation (BP) method. Based on ultrasound images, this technique operates which can be denoted as pre-processing step and segmentation of region of kidney interest in ultrasound images. The authors [15] present an automated approach to delimit the kidneys in CT imageries by means of image processing and CNNs models to minimalizing false positives.

In [16], a potential KT detection is suggested where the input images can be preprocessed through median filter making it noise-free. As well, using principal component analysis (PCA), the attributes were mined which minimalizes the massive collection of variables to the optimum group. Lastly, the image goes through classification using Probabilistic NN where a training dataset was used for making a classified output image finding cancer. In [17], to inspect the performance of different DL approaches here proposed an Adaptive hybridized Deep CNN (AHDCNN) for detecting kidney infection initially and effectively. The efficiency of Classification technology hinges on the dataset role. To increase the classification system accuracy through reduction of the feature dimension, and method was advanced by means of CNN. Such high-level property aids to frame a supervised tissue classifier that would discriminate the two kinds of tissue.

In [18], a hybrid method exploits pre-train model for classification and feature extraction using ML algorithm for the task of kidney disorder image detection. In this work, the pre-trained model applied is the Densenet201 architecture. Sudharson and Kokil [19] develops an automated classification of B-mode kidney ultrasound images by using ensembled DNN using TL. The three different datasets are provided to the SVM for classification afterwards pretrained DNN for feature extraction. The ensembling of pretrained DNNs such as MobileNetV2, ResNet101, and ShuffleNet are integrated and the majority voting method performs final prediction. Sudharson and Kokil [20] present a CAD scheme for identifying multiclass kidney abnormality in ultrasound images. The proposed CAD exploits a pretrained ResNet101 model to extract the feature and SVM classifiers for the classification. Thus, a CAD based method is developed using the despeckling method with the deep residual learning network (RLN) to decrease speckle noise.

DOI: https://doi.org/10.54216/FPA.190230
Received: September 14, 2024 Revised: February 02, 2025 Accepted: March 03, 2025

B. Paper Contributions

This article designs a novel white shark optimizer with ensemble majority voting based kidney cancer classification (WSO-EMVKCC) technique on pathology images. The introduced WSO-EMVKCC model concentrated on the development of a deep convolutional neural network based Xception model for the feature extraction process. Meanwhile, the WSO approach has been used for the optimum hyperparameter tuning of the Xception model. Furthermore, ensemble majority voting classifiers including three ML techniques like long short-term memory (LSTM), sparse autoencoder (SAE), and gated recurrent unit (GRU) methods are employed for kidney cancer classification. The experimental study of the WSO-EMVKCC model is performed on the open access histology image database from the Kaggle repository.

2. Materials and Methods

In this work, we have established a novel WSO-EMVKCC method for the automatic recognition and classification of kidney cancer on pathology images. The presented WSO-EMVKCC technique recognizes the different grades of kidney cancer using DL and ensemble voting concepts. In the proposed WSO-EMVKCC technique, three major processes are included namely Xception-based extraction of features, WSO-based hyperparameter tuning, and ensemble classification. Fig. 1 signifies the working process of WSO-EMVKCC technique.

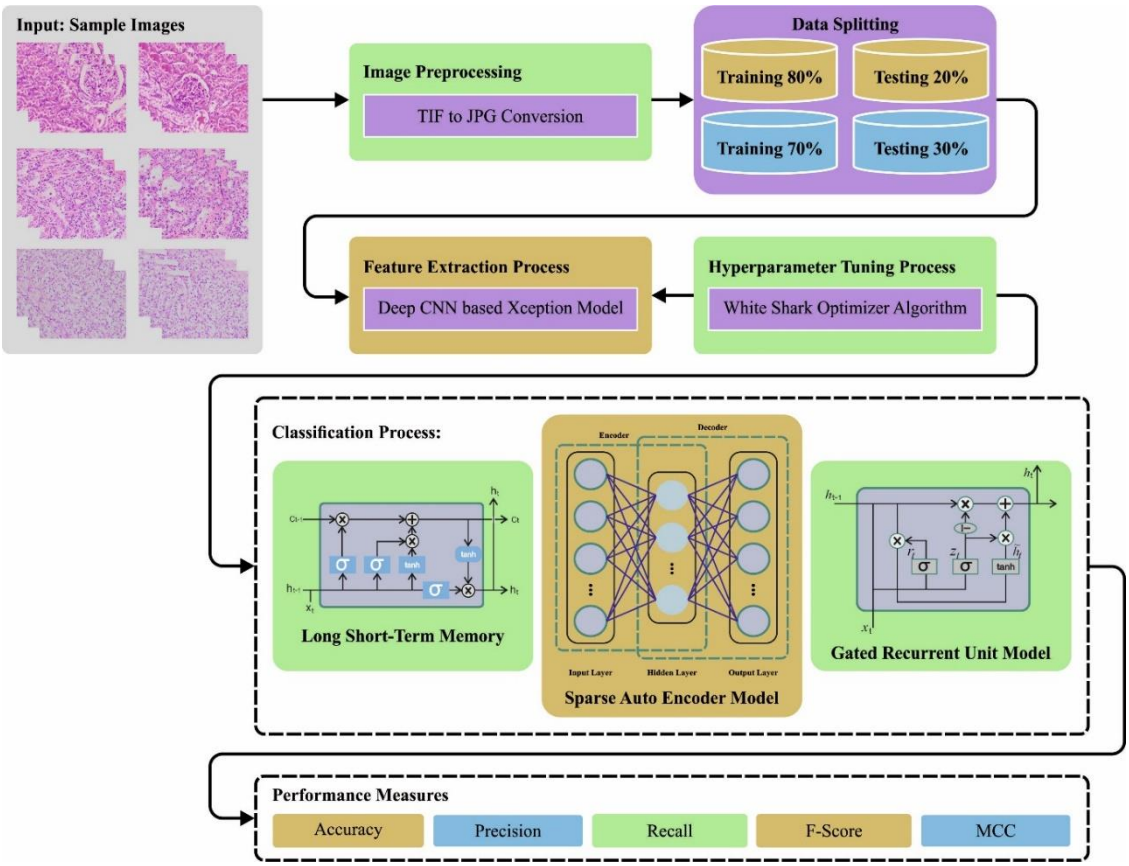

Figure 1. Working process of WSO-EMVKCC approach

A. Xception based Feature Extraction

In the presented WSO-EMVKCC technique, the feature vectors are initially produced by the use of Xception model. Xception is the most effective pretrained model in DL algorithm which mainly depends on the group convolutional layer [21], also called as depthwise separable convolutional layer.

Group Convolutional layer: Here, the input channel is splitted as a collection of groups, and also sliding Conv kernel is employed for this group. In all the groups, this layer convolves; the input arrived and bypasses the kernel of the input vertically and horizontally. Then, the input and the dot product from the weight are evaluated and later add bias function to this layer. This layer independently coordinates the convolution attained from all the groups.

DOI: https://doi.org/10.54216/FPA.190230
Received: September 14, 2024 Revised: February 02, 2025 Accepted: March 03, 2025

The effects of grouped convolutional layer are spatial relationship and cross-channel within the feature maps of the CNN are completely decoupled. The Xception module includes 36 Conv layers, which are ordered into 14 blocks that have linear residual relationships between them, not including initial and final blocks. These 14 blocks are separated into 3 major flows are given below.

Entry Flow: here, the feature was extracted by the 8 Conv layers along with ReLU activation and BN layers. The first 2 Conv layers are typical convolution layers, and the remaining are grouped convolutional layers. The filter in the grouped convolutional layer is double the amount of filters in the typical Conv layer. The amount of filters rises slowly by 2. It begins with 64, followed by128, and later 728

Middle Flow: it extracts complex features by using 24 group convolution layers having 786 filters.

Exit Flow: The most comprehensive feature was extracted by the 4 grouped convolutional layers having filters size 786, 1024, 1536, and 2048, correspondingly. Then, the final Conv layer is used with the size of 3×3 filters, then a global avg pooling layer to reduce the mapping dimension from 3x3 to 1x1, a classification, FC, and Softmax layers.

B. Hyperparameter Tuning using WSO Algorithm

Due to the process of hyperparameter tuning, the WSO technique is applied. The WSO technique is constructed to determine the action of white sharks while searching, which is discussed as follows [22]. Tracking and killing prey are two strategies of WSO. The population of n WSO, in d searching space, with the shark position representing the solution to this problem, as demonstrated in the subsequent $2d$ matrix.

$$w = \begin{bmatrix} w_1^1 w_1^2 & w_2^1 w_2^2 & w_d^1 w_d \\ \therefore & \therefore & \therefore \\ w_1^n & w_2^n & w_d^n \end{bmatrix} \tag{1}$$

Now, w epitomizes the shark location in the search space, d symbolizes the amount of variables selected for the presented. By hearing a pause in the wave, a white shark identifies a location of prey as the prey moves, as follows.

$$u_{k+1}^i = \mu \left[u_k^i + p_1 (w_{gbest_k} - w_k^i) \times c_1 + p_2 (w_{best}^{v_k^i} - w_k^i) \times c_2 \right] \tag{2}$$

where $i = 1,2, \ldots\ldots, n =$ dimension index n, and v^i represents the ith index shark vector getting the optimum position. v_{k+1}^i represent the newest speed vector of ith shark, is signifies in the following:

$$v = \lfloor n \times rand\ (1,n) \rfloor + 1 \tag{3}$$

In Eq. (3), $rand\ (1,n)$ is random number that lies between zero and one.

$$p_1 = p_{\max} + (p_{\max} - p_{\min}) \times e^{-(4k/k)^2} \tag{4}$$

$$p_2 = p_{\min} + (p_{\max} - p_{\min}) \times e^{-(4k/k)^2} \tag{5}$$

From the equations, $p_{\min}$ and pax denote the original and secondary velocity of the white shark motion was set to be 0.5 and 1.5, correspondingly, k represents current and K is maximal iteration,

$$\mu = \frac{2}{|2 - \tau - \sqrt{\tau^2 - 4\tau}|} \tag{6}$$

Where τ indicates the accelerating factor set to 4.125. As defined in Eq. (7), the location updating process was used to define the shark behavior as soon as they approach the prey

$$w_{k+1}^i = \begin{cases} w_k^i . \rightarrow \oplus\ w_0 + u.a + l.b, rand < mv \\ w_k^i + u_k^i / f, rand \geq mv \end{cases} \tag{7}$$

Eqs. (8) and (9), correspondingly, determined a and b as binary vectors.

$$a = sgn(w_k^i - u) > 0 \tag{8}$$

$$b = sgn(w_k^i - 1) < 0 \tag{9}$$

$$w_0 = \oplus\ (a,b) \tag{10}$$

Where $\oplus$ denotes the outcome of bitwise XOR operation. The time gathering of the shark attack the prey and the white shark frequencies wave motion are correspondingly shown in the following:

DOI: https://doi.org/10.54216/FPA.190230
Received: September 14, 2024 Revised: February 02, 2025 Accepted: March 03, 2025

$$f = f_{\min} + \frac{f_{\max} - f_{\min}}{f_{\max} + f_{\min}} \tag{11}$$

$$mv = \frac{1}{(a_0 + e^{(k/2-k)/a_1})} \tag{12}$$

Where a_0 and a_1 denote constant positions used for control exploitation and exploration. Sharks keep the position with the better one who is nearer the prey. Eq. (13) illustrates how this phenomenon can be applied.

$$w'^{i}_{k=1} = w_{gbestk} + r_1 \vec{D}_w sgn(r_2 - 0.5) r_3 < S_s \tag{13}$$

In Eq. (13), $sgn(r_2 - 0.5)$ returns 1 or -1 to adjust the search direction, $w'^{i_{k+1}}$denotes the upgraded position of the shark, D_w denotes the length for both shark and prey and r_1, r_2, and r_3 represent the randomly formed number ranges from 0 to 1. S_s shows the variable that is presented to reflect the power of white shark, as follows:

$$\vec{D}_{\mathrm{w}} = \left| rand \times \left(w_{gbest} - w^i_k \right) \right| \tag{14}$$

$$S_s = \left| 1 - e^{(-a_2 \times k/k)} \right| \tag{15}$$

Where a_2 signifies the factor of location utilized for regulating exploitation and exploration. Algorithm 1, the pseudocode of WSO. The subsequent equation was presented to determine school of white shark fish behaviors:

$$w^i_{k=1} = \frac{w^i_k + w'^{i}_{k+1}}{2 \times rand} \tag{16}$$

In Eq. (16), $rand$ signifies a random integer uniformly distributed within [0,1]. As demonstrated in Eq. (15), the shark can modify their position based on the optimal shark, which has obtained the optimal location, which is close to the prey. The ending position of the shark is somewhere ideally around the target from the searching domain. The cooperative performance of WSO can be recognized by fish actions and the shark movement towards the highest shark and enhanced global and local searching abilities. The WSO approach not only develops a fitness function (FF) to accomplish greater classification performance but also defines a positive integer to describe the better efficiency of the candidate solution. The classification error reduction rate is considered as the FF.

$$fitness(x_i) = ClassifierErrorRate(x_i)$$
$$= \frac{no\ of\ misclassified\ samples}{Total\ no\ of\ samples} * 100 \tag{17}$$

Algorithm 1: Pseudocode of WSO algorithm.

Initialize the parameter of the WSO and the problem

Create the initial position of WSO randomly

Initializing the velocity of population

Estimate the location of the population

while $(k < K)$ do

Upgrade the variables v, p_1, p_2, μ, a, b, w_0, f, m_v and S_s, correspondingly

For $i = 1$ to n do

$$v^{i_{k+1}} = \mu[v^i_k + p_1(w_{gbestk} - w^i_k) \times c_1 + p_2(w'^{v k_{best}} - w^i_k) \times c_2]$$

End for

For $i = 1$ to n do

If $rand < mv$ then

$w^i_{k+1} = w^i_k \cdot - \oplus w_0 + u \cdot a + l \cdot b$

Else

$w^{i_{k+1}} = w^{i_k} + v^{i_k}/f$

End if

DOI: https://doi.org/10.54216/FPA.190230
Received: September 14, 2024 Revised: February 02, 2025 Accepted: March 03, 2025

End for

For $i = 1$ to n do

If $rand \leq S_s$ then

$\overrightarrow{D_w} = |rand \times (w_{gbest} - w_k^i)|$

If $i == 1$ then

$w_{k+1}^i = w_{gbestk} + r_1 \vec{D}_w \text{sgn}\ (r_2 - 0.5)$

Else

$w_{k=1}^{\prime i} = w_{gbestk} + r_1 \vec{D}_w\ \text{sgn}\ (r_2 - 0.5)$

$w_{k=1}^i = \frac{w_k^i + w_{k+1}^{\prime i}}{2 \times rand}$

end if

End if

End for

Modify the location of the white shark that proceeds away from boundary

Estimate and upgrade the novel position

$$k = k + 1$$

End while

Return the optimum solution

C. Image Classification using Ensemble Model

In this study, the ensemble voting classifier can be designed by the use of three ML models such as SAE, GRU, and LSTM. Majority polling is one of the simple and efficient forms of merging the predictions generated through various classifiers. Every class vote was counted in majority voting across the input classifier, and most of the class is chosen [23] Assume a set of training, and a sequence of classifiers as $h_1, h_2, \ldots, h_n$, and each classifier was trained by the training set. Therefore, afterwards training, the classification gives prediction. This classifier h_n generates prediction y_n, classifier h_1, prediction y_1; and classifier h_2, prediction y_2. decreases the voting n class label prediction in the solitary point of data into the single class. Hence, we utilized popular voting for deciding the concluding voting. The operation mode is applied to obtain the resultant vote that is shown.

$$y_f = mode\{h_1(x), h_2(x), \ldots, h_n(x)\} \quad (18)$$

Where $h_i(x) = y_i(x)$.

A. LSTM Model

LSTM network is a recurrent neural network (RNN) type that uses memory block that includes 3 multiplicative components namely forget, input, and output gates and self-connected memory cells, to replace the hidden unit in conventional RNN [23]. The gate allows for resetting, reading, and writing operations and controls behavior of the memory blocks. This enables LSTM network to retain and capture long-term dependency in dataset which make them efficient at modelling complicated temporal dynamics. The input gate, i, enables newest data for entering the memory block:

$$i = sigmoid(W_{ii} * \chi + W_{hi} * h + b_i) \quad (19)$$

W_{ii} and W_{hi} represent the weights that connect the input and prior hidden layer (HL) to input gate. The forget gate, f, removes the prior data stored in the memory block. h indicates the prior HL, χ denotes the input to LSTM unit, and b_i shows the bias term:

$$f = sigmoid\left(W_{if} * \chi + W_{hf} * h + b_f\right) \quad (20)$$

Where $W_i f$ and $W_h f$ denotes the weight that connects the input and prior HL to forget gate and b_f shows the biased term. The output gate, 0, controls to output of the data stored in the memory:

$$0 = sigmoid(W_{io} * \chi + W_{ho} * h + b_0) \quad (21)$$

DOI: https://doi.org/10.54216/FPA.190230
Received: September 14, 2024 Revised: February 02, 2025 Accepted: March 03, 2025

In Eq. (21), The memory cell, c, saves the data from the block of memory. W_{io} and W_{ho} show the weight connects the input and prior HL to output gate and b_0 denotes the bias term. The input and forget gates are updated by Eq. (22):

$$c' = f * c + i * tanh(W_{ic} * \chi + W_{hc} * h + b_c) \tag{22}$$

Here W_{ic} and W_{hc} denote the weight that connects the input and prior HL to a memory cell and b_c represents the bias term. The HL, h, is upgraded by the resultant gate and memory cell:

$$h = 0 * tanh(c') \tag{23}$$

This equation describes the elementary function of a single LSTM unit.

B. GRU Model

The GRU is a variant of RNN that has the benefit of a simple network architecture [24]. Reset and update gates are utilized in GRU for replacing the structure of forget, input, and output gates in LSTM to resolve the problem of gradient explosion and disappearance in RNN, three gates that could decide and judge if the data is fed as output or else. The upgrading gate controls the data of the prior state that is carried to the present state, along with the reset gate controlling the data of the prior position that is expressed to the present candidate state, such that several data pieces are retained and the inappropriate data are removed. The equation of every part of GRU network is given by:

$$r_t = \sigma(W_{xr}x_t + W_{hr}h_{t-1} + b_r) \tag{24}$$

$$z_t = \sigma(W_{xz}x_t + W_{hz}h_{t-1} + b_z) \tag{25}$$

$$\tilde{h}_t = tanh(W_{x\tilde{h}}x_t + W_{hh}(r_t \odot) + b_{\tilde{h}}) \tag{26}$$

$$h_t = z_t \odot \tilde{h}_t + (1 - z_t) \odot h_{t-1} \tag{27}$$

$$y_t = \sigma(W_0 \cdot h_t) \tag{28}$$

Where b_z indicates the biased vector and the upgrading gate is fed with the sigmoid function to attain the gated threshold, W_{xz} and W_{hz} denote the respective weight vector, $b_{\tilde{h}}$ shows the biased vector, and the r_t dimension defines what amount of historical data will be retained. z_t represents the upgrading gate signal demonstrating that the output signal can be organized by upgrade gate signals. $W_{x\tilde{h}}$, $W_{h\tilde{h}}$ represent the weight vector respective to the lattice.

C. SAE Model

A complex structure and training method is deployed, named SAE to attain the best performance and learn abstract and more complex features than traditional AE [25]. Many AE layer was stacked collectively and formed an unsupervised retraining phase whereas the layer of encoder calculated by the AE is utilized as the input to its following AE layer. All the layers are trained like AE by minimalizing the reconstructed error. Once every layer is pre-trained, this network drives to the supervised fine-tuned level. In the supervised fine-tuned stage, add a Softmax layer to the encoded unsupervised layer pre-training phase and discard the decoded layer of SAE. As the amount of units in HLs is larger in the SAE, we imposed a sparse limitation on the HL for capturing higher-level representation. By only keeping a particular set of neurons "active" at all the instances, the sparsity penalty term can be add to the function of loss to avoid identical mapping. In real-time, the neuron is regarded as "active", or else it is "inactive" if the output of a neuron is closer to one and thereby the SAE is transformed into Stacked SAE (SSAE). To accomplish this, add the objective functioned sparse term, which penalizes average activation of $j\text{-}th$ HL ($\hat{\rho}$) once it considerably diverges in the sparsity parameter (ρ):

$$\hat{\rho} = \frac{1}{n}\sum_{i=1}^{n}[f_j(x(i)] \tag{29}$$

$$\rho_{penalty} = \sum_{j=1}^{S} K\,L(\rho||\hat{\rho_j}) \tag{30}$$

Where S represent the amount of neurons in the HL. KL refers to the KullbackLeibler divergence, which can be formulated by:

$$KL(\rho||\hat{\rho}_j) = \rho \log\frac{\rho}{\hat{\rho_j}} + (1-\rho)\log\frac{1-\rho}{1-\hat{\rho_j}} \tag{31}$$

DOI: https://doi.org/10.54216/FPA.190230
Received: September 14, 2024 Revised: February 02, 2025 Accepted: March 03, 2025

In Eq. (31), the objective is that $\hat{\rho}$ closer to a constant ρ, then it is nearer to zero. The sparse penalty term is added to the cost function, it is adapted using Eq. (32):

$$J_{sparse}(\theta) = J(\theta) + \beta \sum_{j=1}^{S} K\, L(\rho || \hat{\rho}_j) \tag{32}$$

3. Results and Discussion

In this article, the stimulation result examination of the WSO-EMVKCC approach can be tested with the Kidney cancer database [26] from Kaggle repository. Table 1 reveals the dataset details. Fig. 2 illustrates the image instances.

Table 1: Details of dataset

Class	No. of Samples
Grade0	45
Grade1	45
Grade2	60
Grade3	67
Grade4	60
Total No. of Samples	277

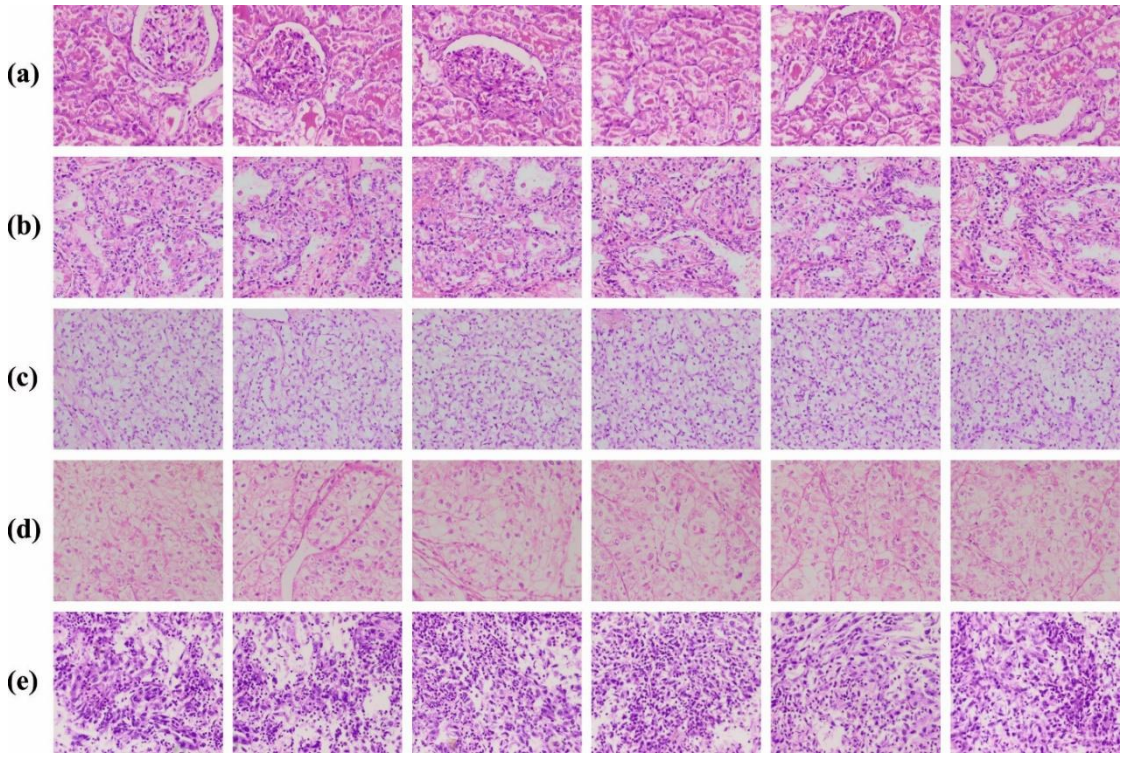

Figure 2. Sample images

In Fig. 3, the confusion matrices of the WSO-EMVKCC technique were depicted. The outcomes indicate that the WSO-EMVKCC technique has properly recognized five classes of kidney cancer.

DOI: https://doi.org/10.54216/FPA.190230
Received: September 14, 2024 Revised: February 02, 2025 Accepted: March 03, 2025

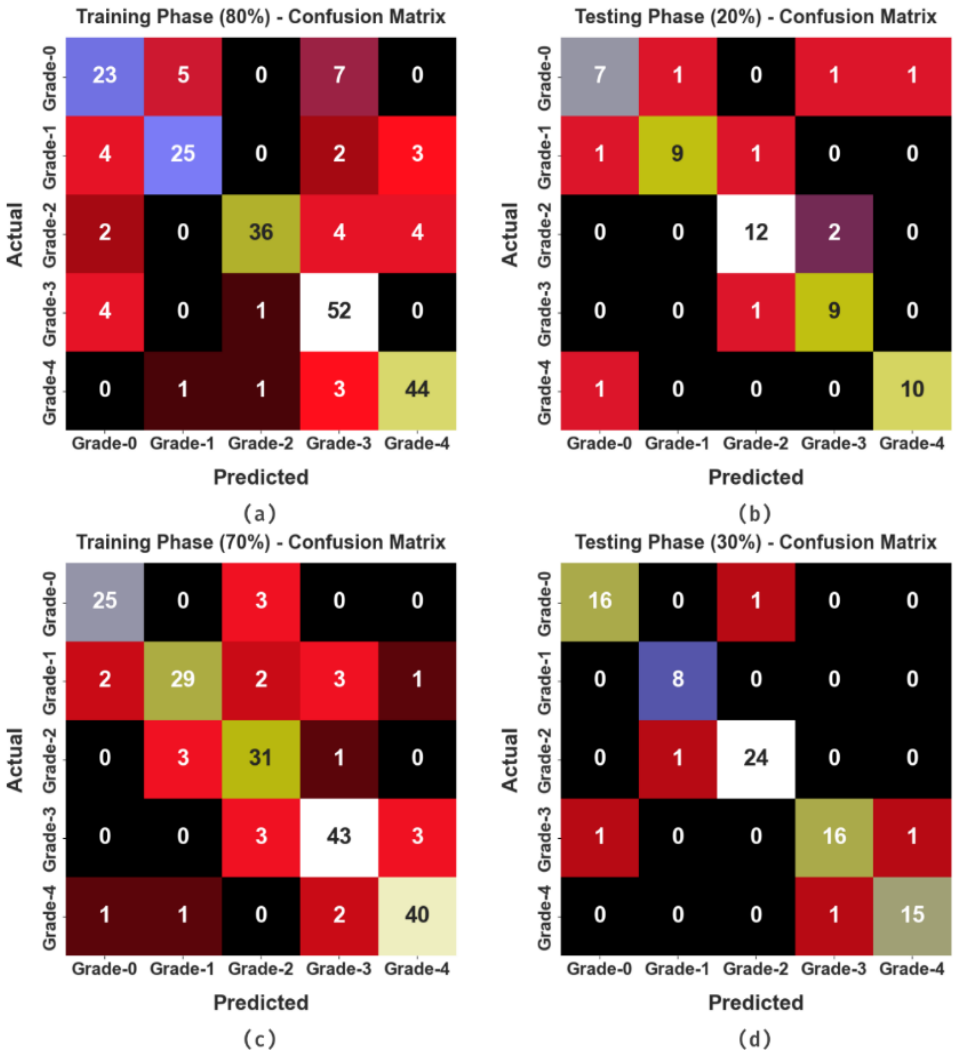

Figure 3. Confusion matrices of WSO-EMVKCC system (a-b) TRP/TSP of 80:20 and (c-d) TRP/TSP of 70:30

Table 2, the complete outcomes of the WSO-EMVKCC model at 80:30 of TRP/TSS. The outcomes demonstrate that the WSO-EMVKCC method attains enhanced results under all classes.

Fig. 4 reports the classification results of the WSO-EMVKCC technique are analysed on 80% of TRP. On grade 0, the WSO-EMVKCC technique attains $accu_y$ of 90.05%, $prec_n$ of 69.70%, $reca_l$ of 65.71%, F_{score} of 67.65%, and MCC of 61.81%. Meanwhile, in grade 2, the WSO-EMVKCC approach accomplishes $accu_y$ of 94.57%, $prec_n$ of 94.74%, $reca_l$ of 78.26%, F_{score} of 85.71%, and MCC of 82.97%. Next, in grade 4, the WSO-EMVKCC methodology reaches $accu_y$ of 94.57%, $prec_n$ of 86.27%, $reca_l$ of 89.80%, F_{score} of 88%, and MCC of 84.52%.

Table 2: Classifier outcomes of WSO-EMVKCC approach on 80:20 of TRP/TSP

Class	$Accu_y$	$Prec_n$	$Reca_l$	F_{Score}	MCC
Training Phase (80%)					
Grade-0	90.05	69.70	65.71	67.65	61.81
Grade-1	93.21	80.65	73.53	76.92	73.06
Grade-2	94.57	94.74	78.26	85.71	82.97
Grade-3	90.50	76.47	91.23	83.20	77.23

DOI: https://doi.org/10.54216/FPA.190230
Received: September 14, 2024 Revised: February 02, 2025 Accepted: March 03, 2025

Grade-4	94.57	86.27	89.80	88.00	84.52
Average	92.58	81.56	79.71	80.30	75.92
Testing Phase (20%)					
Grade-0	91.07	77.78	70.00	73.68	68.46
Grade-1	94.64	90.00	81.82	85.71	82.57
Grade-2	92.86	85.71	85.71	85.71	80.95
Grade-3	92.86	75.00	90.00	81.82	77.92
Grade-4	96.43	90.91	90.91	90.91	88.69
Average	93.57	83.88	83.69	83.57	79.72

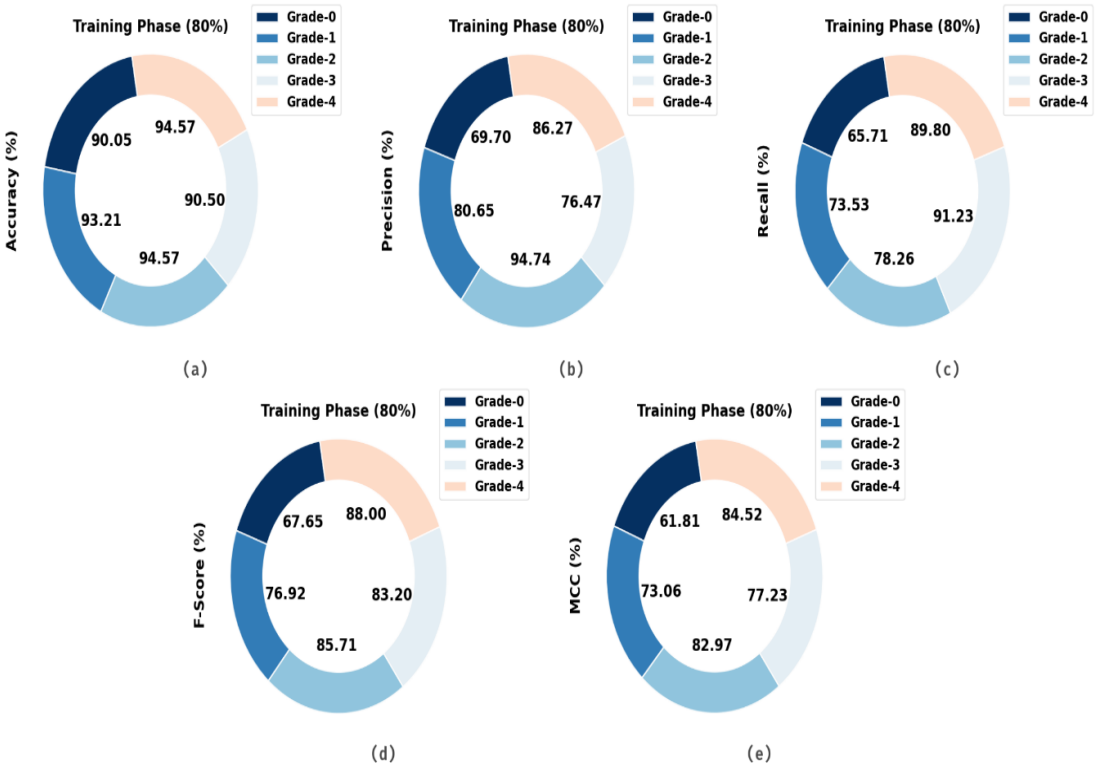

Figure 4. Classifier outcome under 80% of TRP (a) $Accu_y$, (b) $Prec_n$, (c) $Reca_l$, (d) F_{score}, and (e) MCC

Fig. 5 determines the classifier results of the WSO-EMVKCC methodology are examined on 20% of TSP. On grade 0, the WSO-EMVKCC system obtains $accu_y$ of 91.07%, $prec_n$ of 77.78%, $reca_l$ of 70%, F_{score} of 73.68%, and MCC of 68.46%. In the meantime, in grade 2, the WSO-EMVKCC technique reaches $accu_y$ of 92.86%, $prec_n$ of 85.71%, $reca_l$ of 85.71%, F_{score} of 85.71%, and MCC of 80.95%. Afterwards, in grade 4, the WSO-EMVKCC system gains $accu_y$ of 96.43%, $prec_n$ of 90.91%, $reca_l$ of 90.91%, F_{score} of 90.91%, and MCC of 88.69%.

DOI: https://doi.org/10.54216/FPA.190230
Received: September 14, 2024 Revised: February 02, 2025 Accepted: March 03, 2025

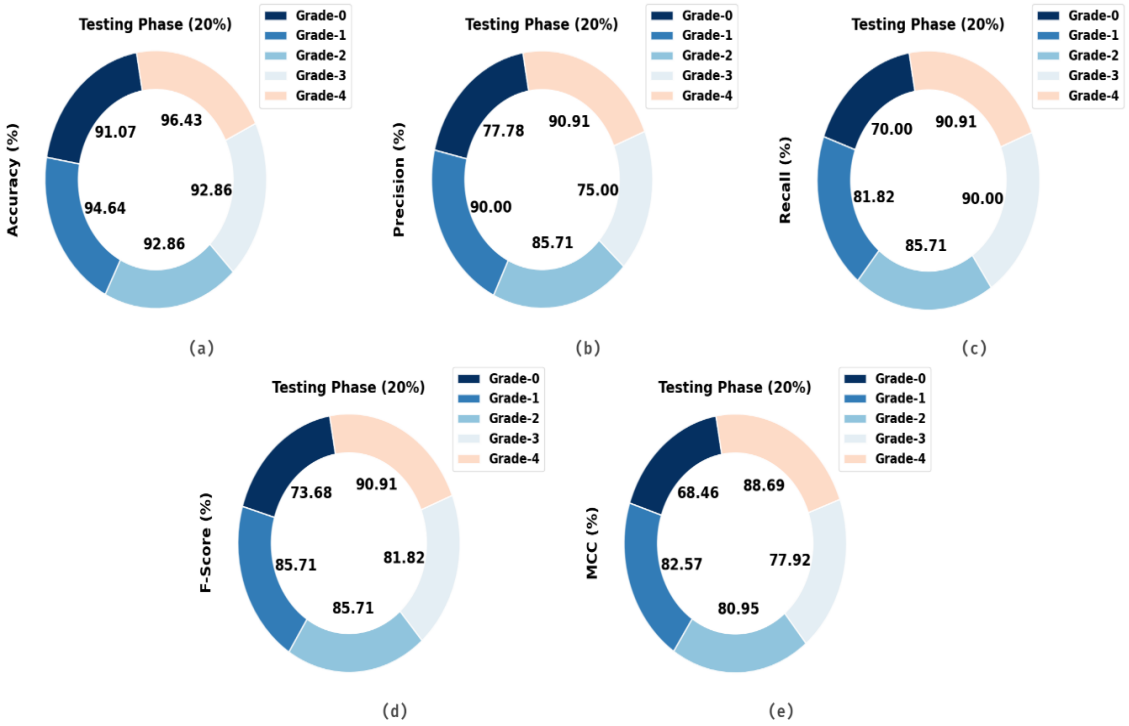

Figure 5. Classifier outcome under 20% of TSP (a) $Accu_y$, (b) $Prec_n$, (c) $Reca_l$, (d) F_{score}, and (e) MCC

Table 3, the complete outcomes of the WSO-EMVKCC technique on 70:30 of TRP/TSS. The results depict that the WSO-EMVKCC approach gains better outcomes on all class labels. Fig. 6 displays the classifier outcomes of the WSO-EMVKCC model analyzed under 70% of TRP. On grade 0, the WSO-EMVKCC technique attains $accu_y$ of 96.89%, $prec_n$ of 89.29%, $reca_l$ of 89.29%, F_{score} of 89.29%, and MCC of 87.47%. Likewise, in grade 2, the WSO-EMVKCC methodology attains $accu_y$ of 93.78%, $prec_n$ of 79.49%, $reca_l$ of 88.57%, F_{score} of 83.78%, and MCC of 80.13%. In addition, in grade 4, the WSO-EMVKCC method attains $accu_y$ of 95.85%, $prec_n$ of 90.91%, $reca_l$ of 90.91%, F_{score} of 90.91%, and MCC of 88.22%.

Table 3: Classifier outcomes of WSO-EMVKCC approach on 70:30 of TRP/TSP

Class	$Accu_y$	$Prec_n$	$Reca_l$	F_{Score}	MCC
Training Phase (70%)					
Grade-0	96.89	89.29	89.29	89.29	87.47
Grade-1	93.78	87.88	78.38	82.86	79.27
Grade-2	93.78	79.49	88.57	83.78	80.13
Grade-3	93.78	87.76	87.76	87.76	83.59
Grade-4	95.85	90.91	90.91	90.91	88.22
Average	94.82	87.06	86.98	86.92	83.74
Testing Phase (30%)					
Grade-0	97.62	94.12	94.12	94.12	92.63
Grade-1	98.81	88.89	100.00	94.12	93.66
Grade-2	97.62	96.00	96.00	96.00	94.31
Grade-3	96.43	94.12	88.89	91.43	89.23
Grade-4	97.62	93.75	93.75	93.75	92.28
Average	97.62	93.37	94.55	93.88	92.42

DOI: https://doi.org/10.54216/FPA.190230
Received: September 14, 2024 Revised: February 02, 2025 Accepted: March 03, 2025

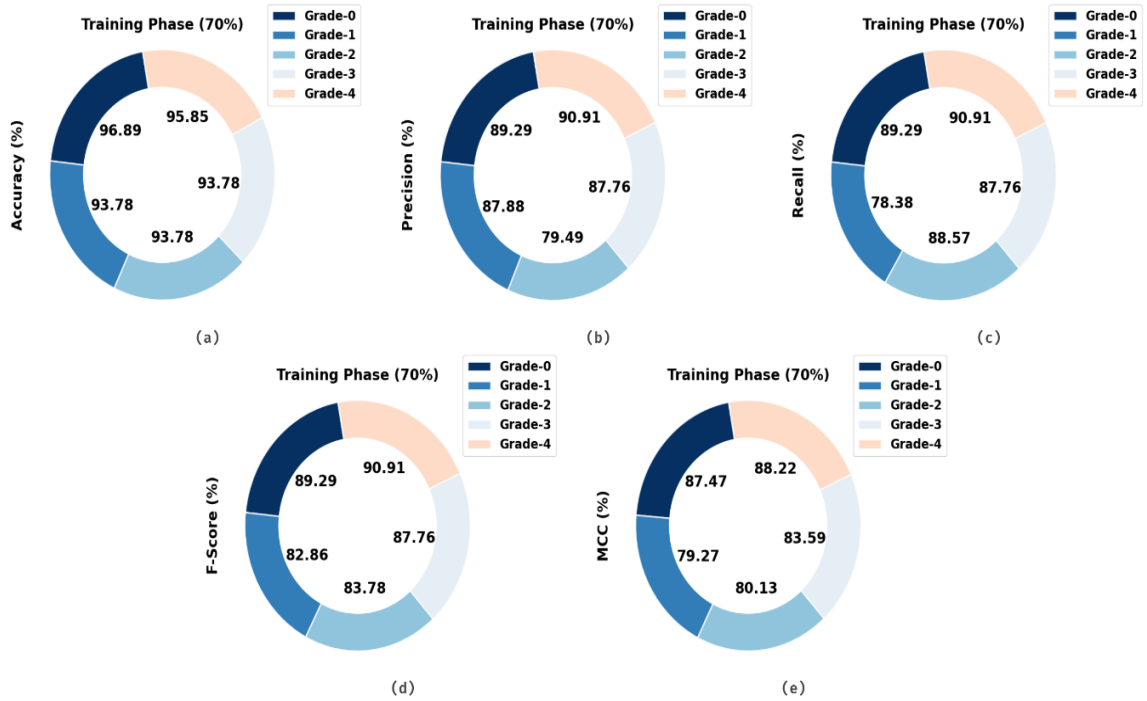

Figure 6. Classifier outcome under 70% of TRP (a) $Accu_y$, (b) $Prec_n$, (c) $Reca_l$, (d) F_{score}, and (e) MCC

Fig. 7 represents the classifier results of the WSO-EMVKCC methodology studied under 30% of TSP. On grade 0, the WSO-EMVKCC technique attains $accu_y$ of 97.62%, $prec_n$ of 94.12%, $reca_l$ of 94.12%, F_{score} of 94.12%, and MCC of 92.63%. Also, in grade 2, the WSO-EMVKCC technique gains $accu_y$ of 97.62%, $prec_n$ of 96%, $reca_l$ of 96%, F_{score} of 96%, and MCC of 94.31%. Next, in grade 4, the WSO-EMVKCC methodology reaches $accu_y$ of 97.62%, $prec_n$ of 93.75%, $reca_l$ of 93.75%, F_{score} of 93.75%, and MCC of 92.28%.

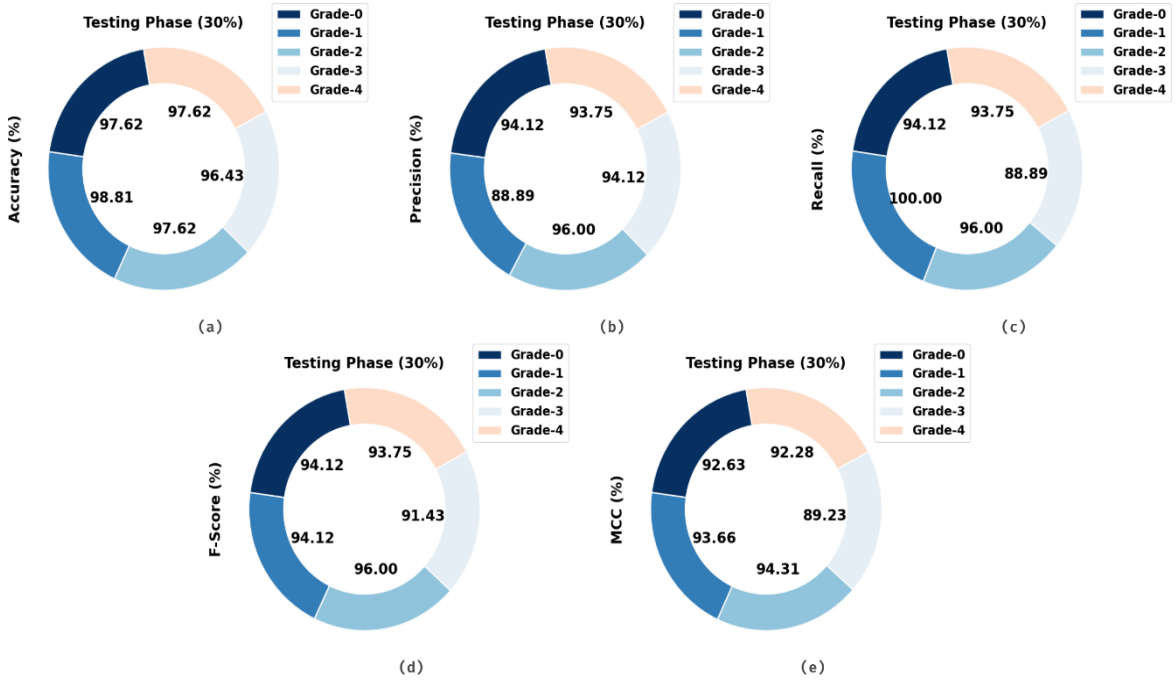

Figure 7. Classifier outcome under 30% of TSP (a) $Accu_y$, (b) $Prec_n$, (c) $Reca_l$, (d) F_{score}, and (e) MCC

DOI: https://doi.org/10.54216/FPA.190230
Received: September 14, 2024 Revised: February 02, 2025 Accepted: March 03, 2025

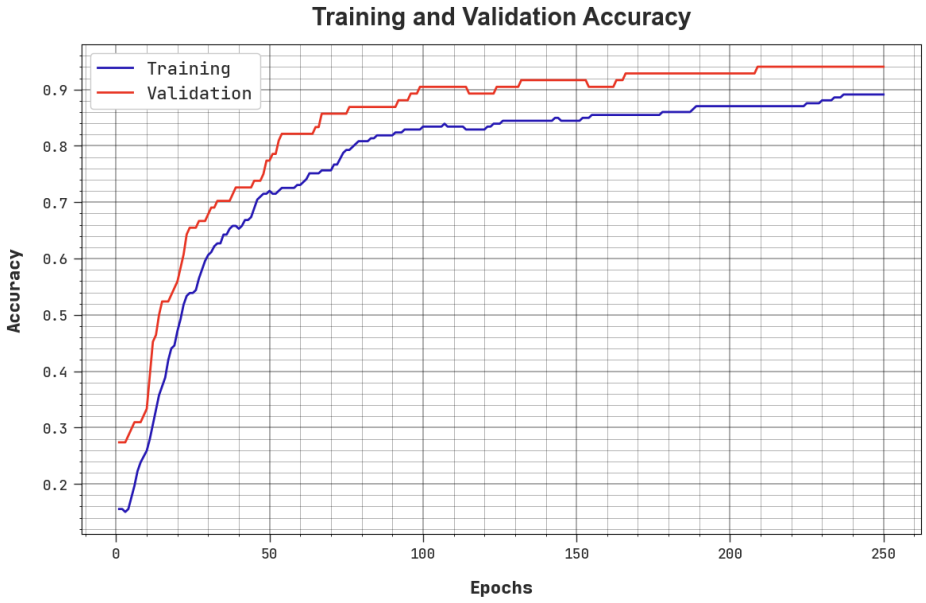

Figure 8. Accuracy curves of WSO-EMVKCC approach

Fig. 8 observes the precision of the WSO-EMVKCC system in the training and validation method on the test database. This figure informs that the WSO-EMVKCC model attains improving precision values across rising epoch counts. Additionally, the growing validation accuracy over training precision shows that the WSO-EMVKCC methodology learns proficiently on the test database.

The loss investigation of the WSO-EMVKCC method at the time of training and validation is defined on the test database in Fig. 9. The results implied that the WSO-EMVKCC system obtains nearer values of training and validation loss. It is detected that the WSO-EMVKCC methodology learns proficiently on the test database.

Figure 9. Loss curves of WSO-EMVKCC approach

In Table 4, a detailed comparison analysis of the WSO-EMVKCC technique with existing approaches is made [12]. In Fig. 10, a comparison of results of the WSO-EMVKCC model under $accu_y$ is given. The results point out that the WSO-EMVKCC model attains better values of $accu_y$. According to $accu_y$, the WSO-EMVKCC system gains higher $accu_y$ of 97.62% whereas the SVM, bagging, ResNet50, KNN, and VGGNet models obtain lower $accu_y$ of 89.17%, 90.64%, 89.60%, 91.12%, and 91.78% correspondingly.

DOI: https://doi.org/10.54216/FPA.190230
Received: September 14, 2024 Revised: February 02, 2025 Accepted: March 03, 2025

Table 4: Comparative outcome of WSO-EMVKCC algorithm with other systems

Methods	$Accu_y$	$Prec_n$	$Reca_l$	F_{Score}
WSO-EMVKCC	97.62	93.37	94.55	93.88
SVM Model	89.17	91.95	90.75	91.35
Bagging Model	90.64	89.77	90.21	89.96
ResNet50 Model	89.60	89.28	90.69	90.92
KNN Model	91.12	89.38	89.51	89.46
VGGNet Model	91.78	91.29	89.42	92.36

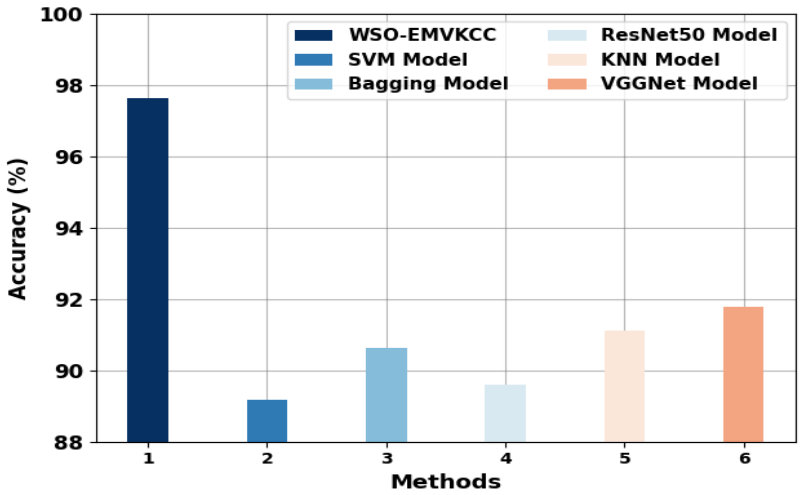

Figure 10. $Accu_y$ Outcome of WSO-EMVKCC algorithm with other systems

In Fig. 11, a comparative outcome of the WSO-EMVKCC algorithm with respect to $prec_n$, $reca_l$, and F_{score} is presented. The outcomes denoted that the WSO-EMVKCC algorithm obtains increasing values of $accu_y$. With respect to $prec_n$, the WSO-EMVKCC technique gains superior $prec_n$ of 93.37% while the SVM, bagging, ResNet50, KNN, and VGGNet systems obtain lower $prec_n$ of 91.95%, 89.77%, 89.28%, 89.38%, and 91.29% correspondingly. Followed by, based on $reca_l$, the WSO-EMVKCC technique gains higher $reca_l$ of 94.55% while the SVM, bagging, ResNet50, KNN, and VGGNet models obtain lower $reca_l$ of 90.75%, 90.21%, 90.69%, 89.51%, and 89.42% correspondingly. At last, interms of F_{score}, the WSO-EMVKCC method gains improve F_{score} of 93.88% while the SVM, bagging, ResNet50, KNN, and VGGNet algorithms reach lesser F_{score} of 91.35%, 89.96%, 90.92%, 89.46%, and 92.36% correspondingly.

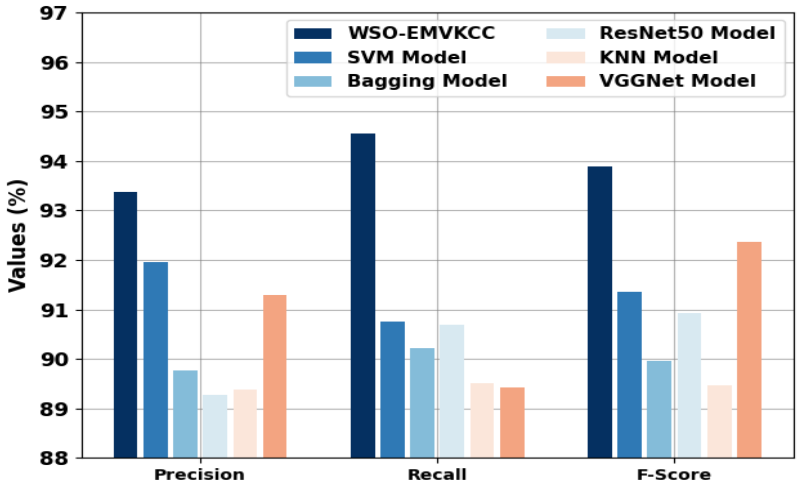

Figure 10. Comparative outcome of WSO-EMVKCC algorithm with other systems

These results ensured the improved performance of the WSO-EMVKCC method over other existing techniques.

DOI: https://doi.org/10.54216/FPA.190230
Received: September 14, 2024 Revised: February 02, 2025 Accepted: March 03, 2025

4. Conclusion

In this article, a new WSO-EMVKCC technique was presented for the automated classification and detection of kidney cancer on pathology images. The presented WSO-EMVKCC model recognizes the different grades of kidney cancer using DL and ensemble voting concepts. In this work, the presented WSO-EMVKCC technique produces the feature vectors using the Xception model, and the WSO algorithm can optimally choose its hyperparameters. Besides, the ensemble majority voting classifier method is developed for the effectual classification and identification of kidney cancer. The stimulated validation of the WSO-EMVKCC method is performed on the open-access histology image database from the Kaggle repository. The stimulated values illustrate the remarkable performance of the WSO-EMVKCC algorithm over other DL techniques

Funding: "This research received no external funding"

Conflicts of Interest: "The authors declare no conflict of interest."

References

[1] A. Abdelrahman and S. Viriri, "Kidney Tumor Semantic Segmentation Using Deep Learning: A Survey of State-of-the-Art," *Journal of Imaging*, vol. 8, no. 3, p. 55, 2022.

[2] K. H. Uhm, S. W. Jung, M. H. Choi, H. K. Shin, J. I. Yoo, S. W. Oh, J. Y. Kim, H. G. Kim, Y. J. Lee, S. Y. Youn, and S. H. Hong, "Deep learning for end-to-end kidney cancer diagnosis on multi-phase abdominal computed tomography," *NPJ Precision Oncology*, vol. 5, no. 1, p. 54, 2021.

[3] M. George and H. B. Anita, "Analysis of kidney ultrasound images using deep learning and machine learning techniques: A review," *Pervasive Computing and Social Networking: Proceedings of ICPCSN 2021*, pp. 183-199, 2022.

[4] J. Guo, W. Zeng, S. Yu, and J. Xiao, "RAU-Net: U-Net model based on residual and attention for kidney and kidney tumor segmentation," in *Proc. 2021 IEEE Int. Conf. Consumer Electronics and Computer Engineering (ICCECE)*, Jan. 2021, pp. 353-356.

[5] M. Lee, S. Wei, J. Anaokar, R. Uzzo, and A. Kutikov, "Kidney cancer management 3.0: can artificial intelligence make us better?," *Current Opinion in Urology*, vol. 31, no. 4, pp. 409-415, 2021.

[6] V. S. Sri, P. S. Kumar, and V. Rajendran, "A Review on Detection of Kidney Disease Using Machine Learning and Deep Learning Techniques," in *Application of Deep Learning Methods in Healthcare and Medical Science*, pp. 1-22, 2022.

[7] M. Gharaibeh, D. Alzu'bi, M. Abdullah, I. Hmeidi, M. R. Al Nasar, L. Abualigah, and A. H. Gandomi, "Radiology imaging scans for early diagnosis of kidney tumors: a review of data analytics-based machine learning and deep learning approaches," *Big Data and Cognitive Computing*, vol. 6, no. 1, p. 29, 2022.

[8] C. H. Hsiao, T. L. Sun, P. C. Lin, T. Y. Peng, Y. H. Chen, C. Y. Cheng, F. J. Yang, S. Y. Yang, C. H. Wu, F. Y. S. Lin, and Y. Huang, "A deep learning-based precision volume calculation approach for kidney and tumor segmentation on computed tomography images," *Computer Methods and Programs in Biomedicine*, vol. 221, p. 106861, 2022.

[9] S. Shubham, N. Jain, V. Gupta, S. Mohan, M. M. Ariffin, and A. Ahmadian, "Identify glomeruli in human kidney tissue images using a deep learning approach," *Soft Computing*, pp. 1-12, 2021.

[10] S. Umamaheswari, D. Sangeetha, C. Mouliganth, and E. M. Vignesh, "KidNet: Kidney Tumour Diagnosis System Design Using Deep Convolutional Neural Network," in *Deep Learning Applications and Intelligent Decision Making in Engineering*, pp. 114-129, IGI Global, 2021.

[11] D. Alzu'bi, M. Abdullah, I. Hmeidi, R. AlAzab, M. Gharaibeh, M. El-Heis, K. H. Almotairi, A. Forestiero, A. M. Hussein, and L. Abualigah, "Kidney Tumor Detection and Classification Based on Deep Learning Approaches: A New Dataset in CT Scans," *Journal of Healthcare Engineering*, 2022.

[12] M. U. Nasir, M. Zubair, T. M. Ghazal, M. F. Khan, M. Ahmad, A. U. Rahman, H. A. Hamadi, M. A. Khan, and W. Mansoor, "Kidney cancer prediction empowered with blockchain security using transfer learning," *Sensors*, vol. 22, no. 19, p. 7483, 2022.

[13] H. S. Shon, E. Batbaatar, K. O. Kim, E. J. Cha, and K. A. Kim, "Classification of kidney cancer data using cost-sensitive hybrid deep learning approach," *Symmetry*, vol. 12, no. 1, p. 154, 2020.

DOI: https://doi.org/10.54216/FPA.190230
Received: September 14, 2024 Revised: February 02, 2025 Accepted: March 03, 2025

[14] F. Ma, T. Sun, L. Liu, and H. Jing, "Detection and diagnosis of chronic kidney disease using deep learning-based heterogeneous modified artificial neural network," *Future Generation Computer Systems*, vol. 111, pp. 17-26, 2020.

[15] L. B. da Cruz, J. D. L. Araujo, J. L. Ferreira, J. O. B. Diniz, A. C. Silva, J. D. S. de Almeida, A. C. de Paiva, and M. Gattass, "Kidney segmentation from computed tomography images using deep neural network," *Computers in Biology and Medicine*, vol. 123, p. 103906, 2020.

[16] A. J. Obaid, "An efficient systematized approach for the detection of cancer in kidney," *International Journal of Scientific and Engineering Research*, vol. 7, no. 1, pp. 1-7, 2020.

[17] G. Chen, C. Ding, Y. Li, X. Hu, X. Li, L. Ren, X. Ding, P. Tian, and W. Xue, "Prediction of chronic kidney disease using adaptive hybridized deep convolutional neural network on the internet of medical things platform," *IEEE Access*, vol. 8, pp. 100497-100508, 2020.

[18] A. M. Qadir and D. F. Abd, "Kidney Diseases Classification using Hybrid Transfer-Learning DenseNet201-Based and Random Forest Classifier," *Kurdistan Journal of Applied Research*, pp. 131-144, 2023.

[19] S. Sudharson and P. Kokil, "An ensemble of deep neural networks for kidney ultrasound image classification," *Computer Methods and Programs in Biomedicine*, vol. 197, p. 105709, 2020.

[20] S. Sudharson and P. Kokil, "Computer-aided diagnosis system for the classification of multi-class kidney abnormalities in the noisy ultrasound images," *Computer Methods and Programs in Biomedicine*, vol. 205, p. 106071, 2021.

[21] M. M. Bassiouni, I. Hegazy, N. Rizk, E. S. A. El-Dahshan, and A. M. Salem, "Automated detection of covid-19 using deep learning approaches with paper-based ECG reports," *Circuits, Systems, and Signal Processing*, vol. 41, no. 10, pp. 5535-5577, 2022.

[22] M. A. Ali, S. Kamel, M. H. Hassan, E. M. Ahmed, and M. Alanazi, "Optimal power flow solution of power systems with renewable energy sources using white sharks algorithm," *Sustainability*, vol. 14, no. 10, p. 6049, 2022.

[23] M. A. Majeed, H. Z. M. Shafri, Z. Zulkafli, and A. Wayayok, "A Deep Learning Approach for Dengue Fever Prediction in Malaysia Using LSTM with Spatial Attention," *International Journal of Environmental Research and Public Health*, vol. 20, no. 5, p. 4130, 2023.

[24] G. Zhang and Y. Lu, "Research on a Lip Reading Algorithm Based on Efficient-GhostNet," *Electronics*, vol. 12, no. 5, p. 1151, 2023.

[25] O. Aouedi, K. Piamrat, and D. Bagadthey, "Handling partially labeled network data: A semi-supervised approach using stacked sparse autoencoder," *Computer Networks*, vol. 207, p. 108742, 2022.

[26] A. Majumdar, "Kidney cancer dataset [Data set]," Kaggle, 2021. [Online]. Available: https://www.kaggle.com/datasets/atreyamajumdar/kidney-cancer.

DOI: https://doi.org/10.54216/FPA.190230
Received: September 14, 2024 Revised: February 02, 2025 Accepted: March 03, 2025